Bespoke Periodic Topography in Hard Polymer Films by Infrared Radiation-Assisted Evaporative Lithography

Argyrios Georgiadis,[a] Alexander F. Routh,[b] M. Murray,[c] and Joseph L. Keddie[a]

[a]Department of Physics and Surrey Materials Institute,
Guildford, Surrey, GU2 7XH United Kingdom
E-mail: j.keddie@surrey.ac.uk

[b]BP Institute, Bullard Laboratories, Madingley Road,
Cambridge, CB3 0EZ United Kingdom

[c]Akzo Nobel Decorative R&D, Wexham Road,
Slough, SL2 5DS, United Kingdom

Abstract

Polymer coatings with periodic topographic patterns, repeating over millimetre length scales, are created from lateral flows in an aqueous dispersion of colloidal particles. The flow is driven by differences in evaporation rate across the wet film surface created by IR radiative heating through a shadow mask. This new process, which we call IR radiation-assisted evaporative lithography (IRAEL), combines IR particle sintering with the concept of evaporative lithography. We show that the height of the surface features increases with an increase in several key parameters: the initial thickness of the film, the volume fraction of particles, and the pitch of the pattern. The results are interpreted by using models of geometry and particle transport. The patterned coatings can function as "paintable" microlens arrays, applicable to nearly any surface. Compared with existing methods for creating textured coatings, IRAEL is simpler, inexpensive, able to create a wide variety of bespoke surfaces, and applicable to nearly any substrate without prior preparation.

Introduction

The topography or texture of a surface[1] – at the micrometer and nanometer length scales – has a profound influence on its properties. For instance, the correct length scales of surface structure can impart hydrophobicity,[2] alter the adhesion,[3-5] reduce the reflectivity of electromagnetic radiation,[6,7] and affect friction and wear.[8]

There have been many recent demonstrations of topographically-patterned coatings in useful applications. As a result of learning from nature, superhydrophobic coatings have been inspired by the texture of the lotus leaf,[9] while antireflection coatings have been inspired by the topography of the moth's eye.[10] In other developments, coatings with topography over a hierarchy of length scales have been found to reduce fouling by marine organisms.[11] Textured coatings have been produced with sub-mm features that reduce the aerodynamic drag on aircraft and hence decrease fuel consumption.[12] Similarly, riblets are known to reduce the hydrodynamic drag on ships.[13] Hierarchically-structured coatings have been used to study the mechanosensitivity of fibroblast cells, with relevance to applications in tissue engineering.[14] In optical applications, surface features have been employed to tune the surface optical band gap,[15] to increase the light extraction efficiency of diodes,[16] and to act as diffraction gratings.[17] Dome-like surface structures function as microlenses.[18] Straining molded and wrinkled surfaces has been used to tune the adhesion of silicone adhesives.[19]

To meet the demands of these myriad applications, there are several techniques[20,21] for creating polymer coatings with topographical structure controlled at length scales of nm or μm. A well established method is photolithography, but it is a multi-step process requiring specially-designed equipment and photosensitive materials. Topographical features, especially ridges, have also been created by wrinkling processes. Wrinkling has been induced by a mismatch of the elastic moduli of surface layers and substrates achieved by the oxidation of silicone,[22] by differences of the thermal expansivity between polymers and metals,[23] and by the swelling of polymers by solvents.[24] This type of coating necessarily requires a

multilayered structure, surface treatments, or a flexible substrate, and hence is not widely applicable.

There are several methods to create topographical patterns in solvent-cast polymer films. For instance, ordered arrays of air bubbles (created when solvent droplets evaporate[25]) have been used to create topographical structures known as breath figures.[26] Elsewhere, less well-ordered topographies have been created from Marangoni instabilities during solvent evaporation from polymer solutions[27] and by surface tension-driven convection.[28] Surface structures can be created in polymers through various types of moulding, such as nano-scale injection moulding,[29] capillary moulding,[30] and ultraviolet nanoimprinting.[31] These techniques have several disadvantages, such as a lack of process flexibility and a need for expensive equipment.

A new direction emerged when Routh and Russel[32] proposed that the modulation of evaporation rate across the surface of a wet colloidal film can drive lateral flow: They placed a mask with holes in it above a latex dispersion. The colloidal polymer particles were carried in the flow towards regions under the holes where water was evaporating fastest. The result was a latex film in which the film was thicker under the pattern of holes in the mask. Building on this work, Harris *et al.* [33] announced a technique, which they named evaporative lithography, which uses holes in masks to modulate evaporation, thereby creating patterns of particles. Water evaporation is faster under the open regions in the mask. A lateral water flux is thus set up to replace the water lost to evaporation. This flux carries particles to the open regions. This team reported a fundamental study of the factors affecting pattern formation from hard particles[33] (polystyrene and silica) and from blends of μm-sized and nm-sized particles.[34] More recently, a new type of evaporative lithography has been used to create dips and rim patterns in very thin colloidal films.[35]

Evaporative lithography presents two limitations. Because a mask blocks most of the wet film surface, the overall evaporation time is greatly increased. For instance, Harris *et al.*[33]

reported that two hours were required to make nanoparticle patterns. Secondly, particles of glassy (hard) polymers, which have a glass transition temperature, T_g, greater than room temperature, are not capable of film formation but yield brittle and cracked coatings.[36] Therefore, patterns cannot be created in hard polymer films using standard evaporative lithography. Recently, a new processing method, called infrared radiation-assisted sintering (IRAS),[37] was demonstrated to be an effective means of processing hard latex films. Heating of polymer particles was achieved by the absorption of infrared radiation, which enabled particle coalescence and film formation in a glassy (i.e. "hard") polymer.

Here, we have merged the techniques of evaporative lithography and IRAS to create patterned coatings from a waterborne dispersion of hard polymer particles. Infrared radiation is shone through the holes in a mask, above a wet latex film, to increase the evaporation rate locally in the exposed areas. Because of the resulting elevated temperatures, drying is faster than in standard evaporative lithography. Particles flow with the water and accumulate under the holes in the mask (Figure 1a). Importantly, the localised heating under the open regions of the mask creates an advantageously strong evaporative flux. Moreover, the infrared heating induces particle sintering and leads to crack-free, hard films with a bespoke topography. We call this new technique infrared radiation-assisted evaporative lithography (IRAEL). We show that IRAEL can create a hard polymer coating with bespoke topography with a pitch, P, able to range from hundreds of μm to a few mm.

Results and Discussion

Figure 1b shows a typical patterned surface, consisting of a square array of dome-like structures, which has been created using IRAEL. Preliminary experiments investigated the effect of the gap height between the mask and initial wet film, h_g (as defined in Figure 1c) on the peak-to-valley height, PV, of the coating's features (defined in Figure 2a). At room temperature, the polymer is hard and glassy, because it is below its T_g of 37.9 °C. Heating via

the NIR radiation facilitates particle sintering[37] and yields a continuous, crack-free film, even in the presence of the mask.

In agreement with results previously reported for evaporative lithography,[33] when the pitch of the mask is fixed, *PV* decreases linearly with increasing h_g, because the evaporation is less confined by a larger gap. See Figure 2b. For the remaining experiments, h_g was therefore fixed at 0.7 mm. This distance was chosen because it is small enough to ensure the technique is effective, yet it does not present practical difficulties.

Systematic studies determined the effect of three important parameters (initial film thickness, h_i, the initial volume fraction of the polymer in the dispersion, ϕ, and the pitch, *P*) in determining the surface topography. In their model of lateral flow in colloidal films, Routh and Russel[32] scaled horizontal distances by the capillary length, given as $L = h_i\left(\frac{\gamma}{3\mu\dot{E}}\right)^{1/4}$, where γ is the surface tension, μ is the dispersion viscosity, and $\dot{E}$ is the evaporation rate, expressed as the velocity at which the surface decreases in height. In the first series of experiments, the initial film thickness was systematically varied. However, to avoid the introduction of other variables in these experiments, the pitch was held constant in normalized units of $L(h_i)$ by fixing the ratio of P:h_i at a value of 6:1. The results in Figure 3a reveal that the peak-to-valley distance increases linearly with the initial film thickness, h_i. This result is expected, because every conceivable length scale in this problem is scaling with h_i.

In a second experiment, when ϕ is increased in the range from 0.09 to 0.37, *PV* likewise increases (Figure 3b). This is understandable, because for a fixed film thickness, there is a greater number of particles with increasing ϕ, which will pile up to create higher peaks. On the other hand, as ϕ increases, the drying time will become shorter. In order to predict the limit at which the drying time, τ_{dry}, is shorter than the time needed for particles to flow to the exposed regions in a mask, τ_{flow}, a normalised time can be defined as $t^* = \frac{\tau_{dry}}{\tau_{flow}}$. The drying

time required to reach a solid-like state is given as $\tau_{dry} = \frac{h_i\left(1 - \phi/\phi_m\right)}{\dot{E}}$, where ϕ_m is the volume fraction at particle close-packing and is taken here to be 0.64.[32] The film will solidify when the particles are packed and hence patterning will not continue when water evaporates at times greater than τ_{dry}. Following the argument of Harris *et al.*,[33] the convection time is given as $\tau_{flow} = \frac{(P - d_h)}{2u}$, where $\frac{(P - d_h)}{2}$ is the distance from the centre of the masked region to a hole edge, and $u = \frac{\dot{E} d_h}{2h_i}$ is the horizontal particle velocity. Combining these equations, t^* is given by $\frac{(1 - \phi/\phi_m) d_h}{P - d_h}$. When $t^* >> 1$, the drying time is long in relation to the time to create patterns, and a patterned surface is expected to result. In these experiments, we estimate that $t^* = 1$ when $\phi \approx 0.32$. With ϕ higher than 0.32, the film will solidify before there is time for it to be patterned, and *PV* is expected to decrease. Such a general trend is indeed observed here; the maximum PV is found at about $\phi = 0.35$. (This argument neglects the effects of particle diffusion, which will counteract the evaporative flow to the unmasked, fast-evaporating regions.)

Finally, when *P* increases from 0.4 mm to 3 mm, with all other parameters fixed, a higher peak-to-valley height results, as is shown in Figure 3c. There is a levelling out in the *PV* values when *P* is greater than 3 mm. This result can be understood from a simple geometric argument (see Electronic Supplementary Information) that conserves the volume of the polymer. As the amount of polymer is fixed, it is not possible for *PV* to increase indefinitely as *P* increases. These results demonstrate that three key parameters can be adjusted to achieve a bespoke topography for specific applications.

A series of experiments was designed to evaluate the effects of modulating the film temperature using IR radiation. Film formation of a soft latex took place under a mask with *P*

= 3 mm and h_g/P = 0.36 under one of three environmental conditions: (1) standard evaporative lithography at room temperature; (2) IRAEL; and (3) with the substrate on a hotplate at 60 °C.

The free evaporation rate of water from the latex, under IR radiation with the same conditions, was measured to be $\dot{E} = 4 \times 10^{-7}$ ms^{-1}. The coating created with IRAEL had the highest *PV* (136.6 ± 6.4 μm) because of this high evaporation rate in the exposed areas, which drives lateral flow of particles. With standard evaporative lithography, a much lower *PV* of 12.7 ± 1.9 μm is obtained because $\dot{E}$ is lower by a factor of 30 compared to the rate under IR heating, and hence the particle flux is reduced. On the other hand, the hotplate promotes fast evaporation across the entire film surface without modulation, so that the lateral flow is reduced. A very low *PV* of 7.1 ± 1.9 μm was obtained. These experiments illustrate the advantage of using IR radiation in obtaining strong topographical patterns. Note that a low T_g latex was used in this experiment, because if the latex with a T_g of 37.9 °C is used at room temperature, particle coalescence is not achieved, and a cracked, opaque film results.

In their study of evaporative lithography from dilute, non-aqueous colloidal dispersions, Harris and Lewis[38] reported the direct observation of Marangoni flows driven by differentials in surface tension arising from the evaporative cooling of the solvent in the unmasked regions. They observed that the recirculation disappeared when the polymer concentration increased above 22 vol. %.

In IRAEL a temperature gradient is established between the masked and unmasked regions. We therefore consider the effects of a temperature-dependent surface tension. A Marangoni flow is expected from the unmasked region into the covered region of the film. Our experimental observation is the opposite, with an accumulation of material under the exposed area. This indicates that any Marangoni flows are less than the induced evaporative flows. To quantify this argument, we consider the lubrication approximation, for surface

tension-driven flow. The characteristic velocity[39,40] is $\frac{\Delta T \frac{d\gamma}{dT}}{\mu}\left(\frac{h_i}{L}\right)$, where ΔT is the temperature drop laterally in the direction of the pitch of the film, and $d\gamma/dT$ is how the surface tension varies with temperature. The characteristic velocity for lateral evaporative flow is $\frac{L\dot{E}}{h_i}$.

Comparing the two velocities defines a dimensionless group, $\psi = \frac{\Delta T \frac{d\gamma}{dT}}{\mu\dot{E}}\left(\frac{h_i}{L}\right)^2 = \Delta T \frac{d\gamma}{dT}\left(\frac{3}{\mu\dot{E}\gamma}\right)^{1/2}$, after substituting for L. For large values of ψ, the Marangoni flow will dominate, whereas for low ψ, the evaporative flux will dominate. If we take $d\gamma/dT$ as -1.5 x 10^{-4} $Nm^{-1}K^{-1}$, which applies for water,[41] and our measured value γ = 0.047 Nm^{-1} for the latex, along with our measured $\dot{E}$ = 4 x 10^{-7} ms^{-1}, we obtain this expression: $\psi \approx 2\Delta T \mu^{-1/2}$, where the dispersion viscosity is measured in Nsm^{-2}. The value of the dispersion viscosity will increase strongly with particle volume fraction, ϕ. The predicted scaling with $\mu(\phi)$ agrees with the findings of Harris and Lewis[38] that at high enough ϕ, the effect of Marangoni flows is small, however at lower ϕ, it must be considered. The extent of contribution from Marangoni flows in IRAEL is currently a topic of further investigation in our laboratory. Nevertheless, for the cases presented here, as we observe the effects of particle transport to the exposed regions, the evaporative flux is dominant.

IRAEL offers the distinct advantages of being simple, inexpensive, single-step, and applicable to substrates without any special preparation. We have applied the process of IRAEL to coatings on a variety of substrates (metal, paper, plastic and glass). A large variety of patterns are possible, limited mainly by the imagination of the mask designer. The radiative heating in the process enables polymer particle sintering[37] of particles with a Tg above room temperature (*i.e.* hard coatings). We anticipate that film formation can be achieved in latex with a T_g as high as 60 °C with the 250 W lamp used here.

Hierarchically structured surfaces can be made through the simultaneous use of masks with two or more pitches. Figure 4a shows an example. Although periodic arrays have been reported here, non-periodic patterns have also been made in our laboratory, including ridged structures and patterns of hemispheres with varying sizes. One practical consideration is that if a large fraction of the mask is covered, then the drying time becomes excessively long (more than 30 minutes).

We have found that the spherical caps reported here can function as microlenses. Periodic arrays of microlenses are widely used in imaging, light projection and light harvesting applications. We envisage "paintable" microlenses and diffusers being applied with IRAEL to any desired surface, such as on street lights, large-area displays, or window panes. Figure 4b shows how a topographically patterned surface is able to concentrate light in a periodic array with a focal length of 14 mm. With control over the pitch and the peak-to-valley heights of the coating surface, it is straightforward to adjust the radius of curvature and hence to adjust the focal length of the lens. For instance, for the surfaces analysed in Figure 3c, the focal length of the lenses increased from 8 mm to 20 mm as the pitch increased from 1.5 mm to 6 mm.

There are numerous methods[42] to fabricate arrays with lens diameters ranging from one to several hundred μm. Arrays of microlenses with diameters in the range from 1 to 2 mm have been previously made via injection molding, hot pressing,[43] excimer-laser irradiation with styrene diffusion,[44] and photothermal effects.[45] Compared to these other methods, IRAEL offers greater flexibility and simplicity. There is great potential to develop other applications for coatings with bespoke topography.

Experimental

Most of the experiments used a latex made through the semi-continuous emulsion polymerization of methyl methacrylate (MMA), butyl acrylate (BA), and methacrylic acid (in

a weight ratio of 18.3:13.3:1), using an ammonium persulfate initiator and an anionic, ethoxylated alcohol surfactant (Rhodafac RK500A, Rhodia).[37] The T_g of the dry latex, measured by differential scanning calorimetry (Q1000, TA Instruments) at a heating rate of 10 °C/min, was 37.9 °C. The average particle diameter, according to photon correlation spectroscopy (Coulter N4 plus, Beckman-Coulter), was 420 nm. The polymer constituted 52 wt.% of the latex, which corresponds to a volume fraction, ϕ, of 0.49, using a density of the copolymer of 1.14 g cm^{-3} (estimated using the reported densities of poly(methyl methacrylate)[46] and poly(butyl acrylate)[47]) In some experiments, ϕ was decreased by dilution with deionised water and increased by evaporation of the water while stirring. The surface tension of the latex was measured by the Wilhelmy plate method using a commercial tensiometer (Nima Technology Ltd. Coventry). Some experiments used a second acrylic copolymer latex (mean diameter of 420 nm), which was made with a higher BA:MMA ratio leading a T_g of 13 °C.

Masks were made from steel plates (1.5 mm thick) in which holes with a diameter d_h were spaced in a square array with a fixed centre-to-centre distance, or pitch, P. The masks were placed on a holder above a wet film, which was cast on a glass substrate from a micropipette and spread uniformly. The initial thickness of the wet latex film, h_i, was adjusted by depositing the required mass of wet latex across a known area. The distance between the film surface and the bottom of the mask, called the gap height, h_g, was controlled through the use of digital callipers attached to a mask holder to move vertically the required distance. In a typical experiment, a 250 W near IR lamp (Model 470 IR, Interhatch) was placed 16.5 cm above the mask. The temperature of the film during the IRAEL process was recorded using a thermocouple wire attached to the substrate and in contact with the wet latex film. Within 20 min the temperature rose from 22 °C to 70 °C. Thereafter, the polymer layer reached a maximum temperature of 80 °C, which is well above the polymer's T_g of 37.9 °C.

Topographical features, including the peak-to-valley height, were measured by stylus profilometry (Dektak 8, Veeco) with a stylus force in the range between 100 and 150 μN. The mean of nine or more measurements is reported. A series of masks was produced with P in the range from 400 μm to 7 mm, while maintaining a constant ratio of P:d_h of 3:2, so that in all masks 35% of the area was open.

Acknowledgements

A.G. acknowledges a Ph.D. studentship from the UK Engineering and Physical Sciences Research Council (EPSRC) and Akzo Nobel. We benefitted from useful discussions with Phil Beharrell and John Jennings (Akzo Nobel). Alexander Nicholas (University of Kent) performed some preliminary experiments with funding from a summer bursary from the South East Physics Network (SEPNet). Violeta Doukova provided laboratory assistance.

References

1 X. Jiang, P. J. Scott, D. J. Whitehouse, L. Blunt, *Proc. Roy. Soc. A*, 2007, **463**, 2049.

2 S.M. Lee, T. H. Kwon, *Nanotechnology*, 2006, **17**, 3189.

3 E. Verneuil, B. Ladoux, A. Buguin, P. Silberzan, *J. Adhesion*, 2007, **83**, 449.

4 C. Poulard, F. Restagno, R. Weil, L. Léger, *Soft Matter*, 2011, **7**, 2543.

5 K.N.G. Fuller, D. Tabor, *Proc. R. Soc. London, Ser. A*, 1975, **345**, 327.

6 J. Lekner, *Theory of Reflection: Of Electromagnetic and Particle Waves*, Springer, Dordrecht, Netherlands, **1987**, Ch. 11.

7 J. S. Rayleigh, *Proc. Lond. Math. Soc*., 1880, **11**, 51.

8 U. Pettersson, S. Jacobson, *Tribology International*, 2003, **36**, 857.

9 W. Ming, D. Wu, R. van Benthem, G. de With, *Nano Letters*, 2005, **5**, 2298.

10 P.B. Clapham, M.C. Hutley, *Nature*, 1973, **244**, 281.

11 K. Efimenko, J. Finlay, M. E. Callow, J. A. Callow, J. Genzer, *Appl. Mater. Interf*., 2009, **1**, 1031.

12 V. Stenzel, Y. Wilke, W. Hage, *Prog. Org. Coat.*, 2011, **70**, 224.

13 S. Gogte, P. Vorobieff, R. Truesdell, A. Mammoli, F. van Swol, P. Shah, C. J. Brinker, *Phys. Fluids*, 2005, **17**, 051701.

14 H. Vandeparre, S. Gabriele, F. Brau, C. Gay, K. K. Parker, P. Damman, *Soft Matter*, 2010, **6**, 5751.

15 S. F. Ahmed, G.-H. Rho, K.-R. Lee, A. Vaziri, M.-W. Moon , *Soft Matter*, 2010, **6**, 5709.

16 J. Rao, R. Winfield, L. Keeney, *Opt. Comm*., **2010**, *283*, 2446.

17 N. Bowden, W. T. S. Huck, K. E. Paul, G. M. Whitesides, *Appl. Phys. Lett*., 1999, **75**, 2557.

18 D. Chandra, S. Yang, P. Lin, *Appl. Phys. Lett*., 2007, **91**, 251912.

19 H.E. Jeong, M.K, Kwak, K.Y. Suh, *Langmuir*, 2010, **26**, 2223.

20 E. Menard, M. A. Meitl, Y. Sun, J.-U. Park, D. J.-L. Shir, Y.-K. Nam, S. Jeon, J. A. Rogers, *Chemical Reviews*, 2007, **107**, 1117.

21 Z. Nie, E. Kumacheva, *Nat. Mater.*, 2008, **7**, 277.

22 A. Chiche, C. M. Stafford, J. T. Cabral, *Soft Matter*, 2008, **4**, 2360.

23 N. Bowden, S. Brittain, A. G. Evans, J. W. Hutchinson, G. M. Whitesides, *Nature*, 1998, **393**, 146.

24 S. Yang, K. Khare, P. C. Lin, *Adv. Funct. Mat.*, 2010, **20**, 2550.

25 M. Srinivasarao, D. Collings, A. Philips, S. Patel, *Science*, 2001, **292**, 79.

26 U.H.F. Bunz, *Adv. Mater.*, 2006, **18**, 973.

27 N. Bassou, Y. Rharbi, *Langmuir*, 2009, **25**, 624.

28 S. Xu, M. Li, Z. Mitov, E. Kumacheva, *Prog. Org. Coat.*, 2003, **48**, 227.

29 S. H. Kim, J.H. Jeong, J.R. Youn, *Nanotechnology*, 2010, **21**, 205302.

30 E. Kim,Y. Xia, G. M. Whitesides, *Nature*, 1995, **376**, 581.

31 S. Jeon, J.-W. Kang, H.-D. Park, J.-J. Kim, J. R. Youn, J. Shim, J.-H. Jeong, D.-G. Choi, K.-D. Kim, A. O. Altun, S.-H. Kim, Y.-H. Lee, *Appl. Phys. Lett.*, 2008, **92**, 223307.

32 A. F. Routh, W. R. Russel, *AIChE Journal*, 1998, **44**, 2088.

33 D. J. Harris, H. Hu, J. C. Conrad, J. A. Lewis, *Phys. Rev. Lett.*, 2007, **98**, 148301.

34 D. J. Harris, J. C. Conrad, J. A. Lewis, *Phil. Trans. Roy. Soc. A*, 2009, **367**, 5157.

35 C. Parneix, P. Vandoolaeghe, V. S. Nikolayev, D. Quéré, J. Li, B. Cabane, *Phys. Rev. Lett*. 2010, **105**, 266103.

36 J. L. Keddie, A. F. Routh, *Fundamentals of Latex Film Formation: Processes and Properties*, Springer, Dordecht, 2010, Chapter 1.

37 A. Georgiadis, P. A. Bryant, M. Murray, P. Beharrell, J. L. Keddie, *Langmuir*, 2011, **27**, 2176.

38 D. J. Harris, J. A. Lewis, *Langmuir*, 2008, **24**, 3681.

39 D. P. Gaver, J. B. Grotberg, *J. Fluid Mech*., 1992, **235**, 399.

40 V. R. Gundabala, C.-H. Lei, K. Ouzineb, O. Dupont, J. L. Keddie, A. F. Routh, *AIChE J*, 2008, **54**, 3092.

41 N. B. Vargaftik, B. N. Volkov, L. D. Voljak, *J. Phys. Chem. Ref. Data*, 1983, **12**, 817.

42 J.Y. Huang, Y.-S. Lu, J.A. Yeh, *Optics Express*, 2006, **14**, 10779.

43 P. Pantelis, D. J. McCartney, *Pure Appl. Opt*., 1994, **3**, 103.

44 S. Lazare, J. Lopez, J. Turlet, M. Kufner, S. Kufner, P. Chavel, *Appl. Opt*., 1996, **35**, 4471.

45 S. Calixto, G. P. Padilla, *Appl. Opt*., 1996, **35**, 6126.

46 W. G. Gall, N. G. McCrum, *J. Polym. Sci*., 1961, **50**, 489.

47 D. W. Van Krevelen, *Properties of Polymers*, Elsevier, Amsterdam,1990, p. 70.

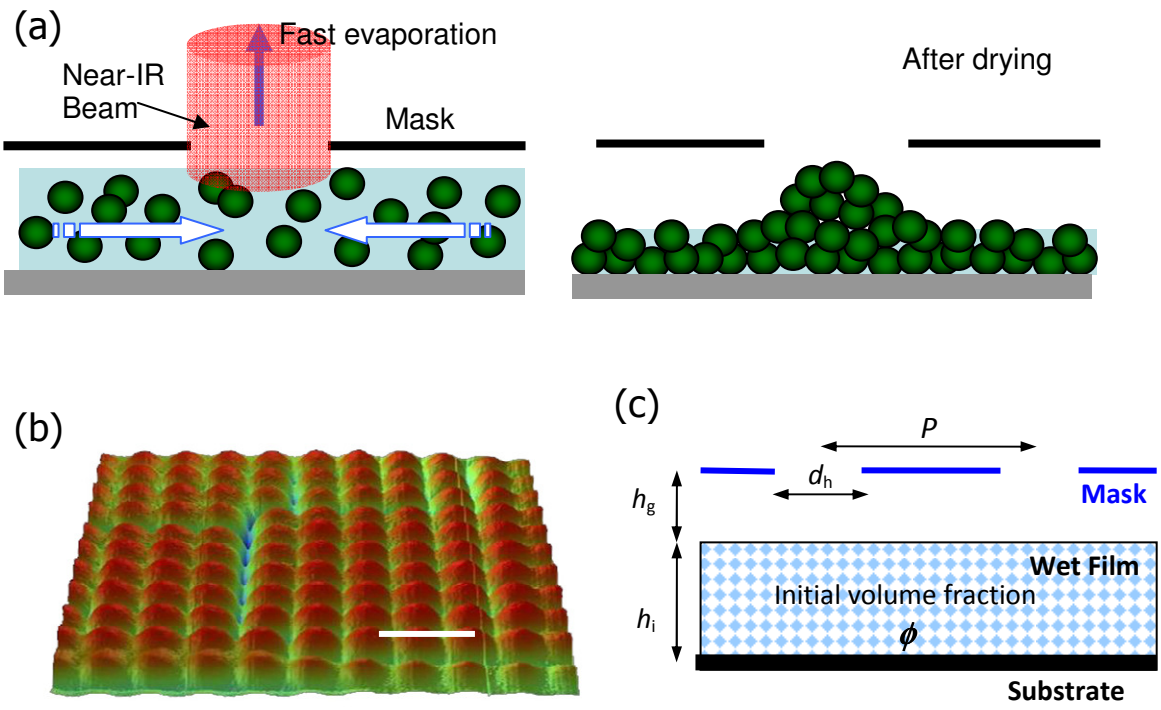

Fig. 1 (a) Overview of the IRAEL process: A colloidal film is placed under a mask. IR radiation heats the wet film in the exposed areas. Particles flow with the water and accumulate under the holes in the mask and sinter as a result of heating. (b) A profilometry image (1.5 cm x 1.5 cm) shows the dome-like features of a patterned polymer film created by IRAEL. Here, P = 1.5 mm, h_g = 0.7 mm, and h_i = 0.33 mm. Scale bar is 3 mm. (c) Definition of relevant experimental parameters in IRAEL: h_g, h_i, d_h, P, and ϕ.

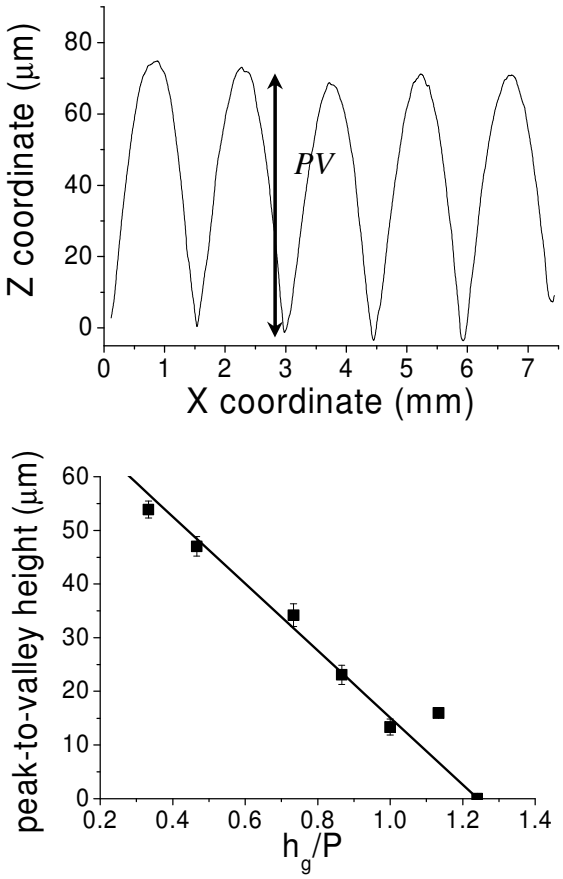

Fig. 2 (a) An example of a profilometry line scan of the surface presented in Figure 1b. The peak-to-valley height, *PV*, is defined as the vertical distance between the minimum height between neighbouring features and the maximum height of those features. (b) *PV* values of patterned surfaces, measured as a function of increasing gap height, h_g, when *P* is fixed at 1.5 mm.

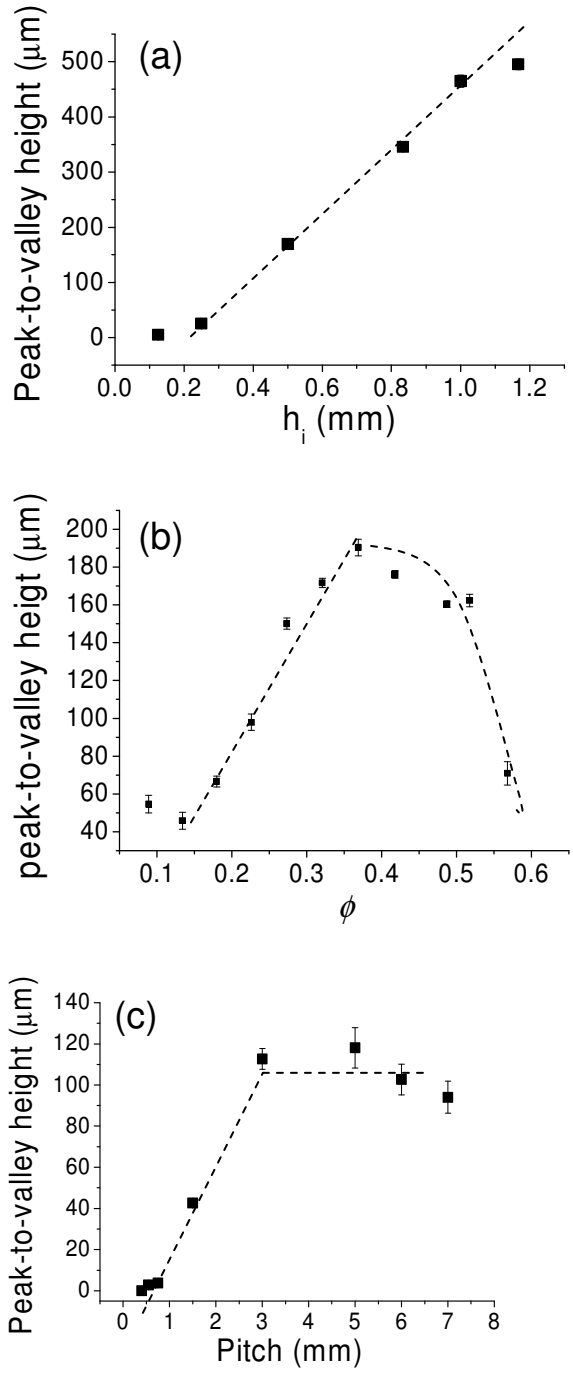

Fig. 3 Dependence of the peak-to-valley heights on key parameters. (a) The initial film thickness, h_i, when the ratio of P:h_i is fixed at 6:1; (b) the solids content, ϕ, of the latex, with fixed h_i = 470 μm and P = 3 mm; and (c) the pitch of the masks, with h_i fixed at 330 μm. The dashed lines are guides for the eye.

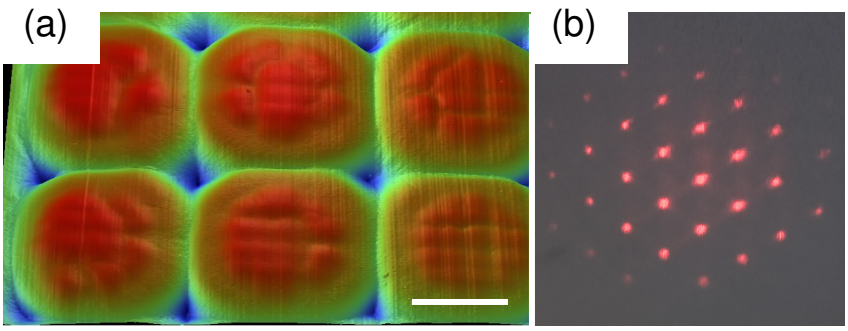

Fig. 4 (a) Profilometry image of a hierarchically-structured surface created by IRAEL using the superposition of two masks with different pitches (P=7 mm and P=1.5 mm) with an initial film thickness of 0.26 mm. Each spherical cap has a period texture imposed on it. Scale bar is 3.5 mm. (b) Photograph of a periodic array of focused points of light obtained by projection of an expanded HeNe laser beam through a topographically patterned coating on glass. In the IRAEL for this surface P = 4 mm, h_i = 0. 7 mm.